



Friction Stir Additive Manufacturing of AA7075/Al₂O₃ and Al/MgB₂ Composites for Improved Wear and Radiation Resistance in Aerospace Applications

R. Srinivasan^{1*}, Amuthakkannan Rajakannu², S. Rajesh³, J. Sathees Babu⁴, G. Dinesh⁴ and S. Mayakannan⁵

¹Department of Mechanical Engineering, KGiSL Institute of Technology Saravanampatti, Coimbatore, TN, India

²Department of Mechanical and Industrial Engineering, College of Engineering, National University of Science and Technology, Muscat, Oman

³Department of Mechanical Engineering, Meenakshi college of Engineering, Chennai, TN, India

⁴Centre for Material Science, Vinayaka Mission's Kirupananda Variyar Engineering College, Salem, TN, India

⁵Department of Mechanical Engineering, Rathinam Technical Campus, Coimbatore, TN, India

Received: 03.11.2024 Accepted: 10.03.2025 Published: 30.03.2025

*vlbsrini@gmail.com



ABSTRACT

The research focuses on a class of materials called multifunctional metal matrix composites (MMCs) that combine with structural and functional characteristics. These materials can offer better protection from space environmental dangers without sacrificing scalability, weight, or mass. An MMC is a metal matrix composite made using a scalable friction stir additive manufacturing (FSAM) technique. It contains more than 30% volume of evenly distributed metallic/ceramic particles. In aluminum MMCs, the FSAM approach and the significant amount of nanoparticles significantly improve the microstructures of the metal matrices, leading to interparticle gaps smaller than 1 μm . So, the FSAM process refines the MMC matrix while combining a high concentration of metallic and ceramic particles. This improves hardness and coefficient of friction, and it also integrates the functionalities of adding nanoparticles into the MMCs, which is crucial for justifying threats in the aviation environment. This allows for effective radiation shielding, increased durability in high temperatures, and increased friction at contact surfaces.

Keywords: Friction stir additive manufacturing; AA7075; Nanoparticles; Microstructure; Hardness.

1. INTRODUCTION

Space exploration including low-Earth orbit satellite operations, interplanetary flight, and living on the Moon or Mars has consistent hurdles in protecting persons and equipment from diverse environmental risks and threats. Additive manufacturing (AM) technologies significantly influence the fourth industrial revolution. FSAM is an innovative solid-state technique that circumvents the metallurgical challenges associated with the most available techniques, which entail melting and solidification (Venkit and Selvaraj, 2022; Sharifzadeh *et al.* 2024). Metal additive manufacturing methods have the potential to produce intricate parts, rendering them a viable option for the automotive, space, and naval sectors (Choudhury *et al.* 2023). The new solid-state method that builds on the foundation of the FSW process is FSAM. Unlike traditional fusion welding, FSW eliminates welding flaws when used to unite incompatible metals (Nallusamy *et al.* 2024). The fundamental principles of additive manufacturing and FSW are initially presented to establish the necessity and notion of friction-based additive techniques (FATs). The next step is giving each FAT its guiding principles and specific benefits

(Srivastava *et al.* 2019). A solid-state AM method, FSAM yields a microstructure that is both controllable and homogeneous, as well as exceptional structural performance (Kundurti and Sharma, 2023). The different pin profiles significantly influence material flow, microstructural characteristics, and overall performance of the manufactured components. The FSAM method is used to create large structures with expected mechanical properties and without defects. As a result, the newly made composite can replace the traditional material used in car parts (Venkit and Selvaraj, 2022). Using FSAM, a three-layer structure was created by 3 mm thick AA7075-T6 and AA5083 alloys for the top and bottom layers, respectively. When compared to base metal (AA5083), the build's upper and lower regions exhibit significantly higher levels of strength and microhardness (Jha *et al.* 2023a). Compared to the unreinforced composites, the AA5083/AA6061/SiC composite achieved a significantly higher maximum strength of 291 MPa.

Nano-scaled metal borides have recently begun to be utilized in sustainable technologies, and we offer our insights on the future direction of this topic (Chakrabarty *et al.* 2023). The oxidation/combustion of

MgB₂ within the paraffin was delineated by 4-step oxidation progress happening from 473 K to 1723 K. There was an analysis of four oxidation pathways and a proposal for a combustion model including MgB₂ contained in a matrix (Pal *et al.* 2023). The extremely low resistance and excellent efficiency of MgB₂ make it a striking material for use in microchip technology and medicine. The findings of the morphological examination revealed a crystalline grain structure and consistent deformation without fractures (Herbirowo *et al.* 2023). MgB₂ ceramics have been extensively studied due to their remarkable superconducting capacity at 39 K transition temperature. (Prakasam *et al.* 2020). Adding MgB₂ and intermetallic phases caused by annealing significantly increases hardness (up to 6) and promotes hydrophilicity and antibacterial properties in the coating (Bülbül and Kara, 2024).

Mechanical testing has shown that agglomerate particle cracking affects tensile ductility relative to the base alloy. Better processing procedures are needed to break up oxide particle clusters and make them more equally dispersed following laser exposure. (Lopez *et al.* 2023). Second-phase particles created by additive manufacturing are thought to be responsible for the alloy's exceptional radiation resistance by maintaining thin cell borders (Aydogan *et al.* 2022). The as-built microstructure of this 316 L material may be responsible for its higher radiation resistance. Cellular sub-grain boundaries, undissolved particles, and delta ferrite grains create an environment where defects are less likely to migrate. (Hawkins *et al.* 2023). The microstructural study and thermal-mechanical performance of the samples proved that the SiC matrix combined with TRi-structural ISotropic (TRISO) fuel, which was created using AM technology, was technically feasible and had enhanced capabilities (Lu *et al.* 2024).

Raw sheets of AA5083 varied in thickness from the previous layer at a rate of 0.8 mm. The order of the layers was 3, 2, 2.5, and 1.5 mm in terms of thickness. (Tagimalek and Mahmoodi, 2023). A combination of experimental and numerical methods is used to study the physical mechanism of performance increase of FSAM-produced nanoparticle-reinforced aluminum matrixes. Adding dispersed Al₂O₃ nanoparticles to composite layers increases toughness and decreases average grain sizes (Tan *et al.* 2021). The AA6061-T6 additively manufactured components have several desirable properties, such as a hardness of approximately 60 HV, a wear rate of roughly 3 µgr/Nm, a friction coefficient ranging from 0.6 to 0.8, and a corrosion rate below 5 mph (Kiani *et al.* 2024). The study analyzes microstructural changes, hardness distribution, and wear characteristics on two different surfaces using two different rotational speeds (800 rpm and 1200 rpm), traverse rates (41 mm/min and 82 mm/min), and a 50% pin overlap during block production (Das *et al.* 2024). Applications in various industrial sectors and the capacity to weld similar

and dissimilar materials are affected by the changes in input reactions, which modify the microstructure, hardness, and strength of the welded joints (Bhattacharjee *et al.* 2023).

This work advances metal matrix composites (MMCs) by using Friction Stir Additive Manufacturing (FSAM) to achieve high ceramic loading (>30%), uniform microstructures (<1 µm interparticle spacing), and superior mechanical properties like higher hardness (~180 HV) and wear resistance. Unlike traditional methods, FSAM enables scalable, defect-free, thin-wall MMC fabrication at a high build rate (>1080 cm³/h). Additionally, these MMCs offer enhanced radiation shielding (25-40% improvement over aluminum) and improved friction and impact resistance, making them ideal for space and aerospace applications.

A scalable stacked FSAM composite with a maximum proportion of ceramic particles was investigated in this study as a potential composite to enhance protection against space environment hazards, including ionizing radiation shielding and impact resistance. Investigating AMMCs supplemented with ceramic powder started with various microstructural assessment methodologies, like scanning electron microscopy (SEM) fixed with energy dispersive spectroscopy (EDS). Microstructures were correlated with the capabilities needed for space applications through hardness tests, wear testing, photon radiation evaluations, and modeling relevant to low Earth orbit (LEO) radiation settings.

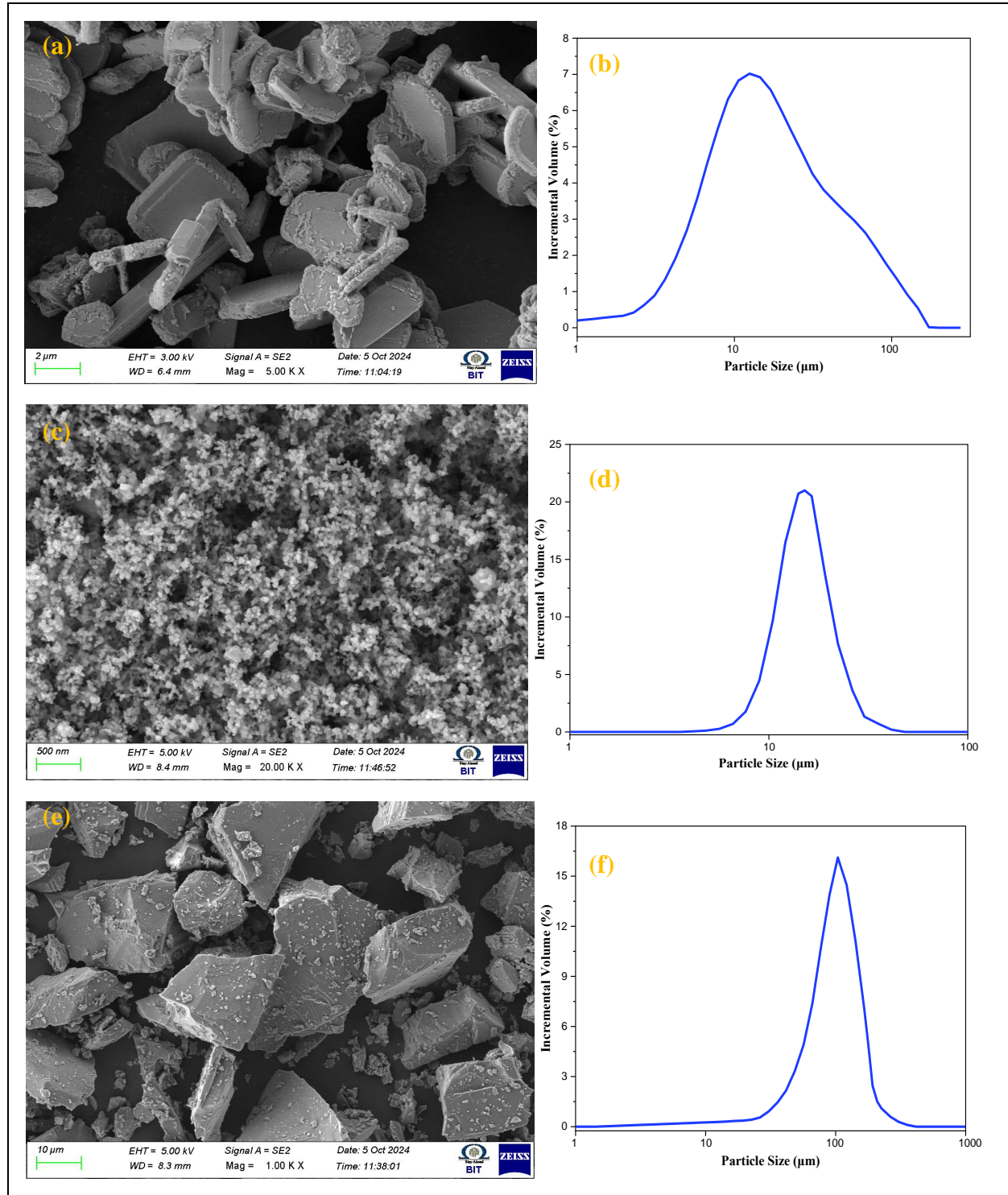
2. MATERIAL AND METHODS

Fig. 1 shows that the stacked FSAM method uses ceramic materials such as alumina and magnesium diboride (MgB₂) to reinforce AMMCs. There is a lot of clustering and irregular particle shapes in the MgB₂ particle feedstock. Half of the agglomerates (d₅₀) have a size smaller than 14 µm, and the particle size of the MgB₂ clumps is quite extensive, between 1 and 140 µm (Fig. 1b). The study found a correlation between the feedstock particle size and the resulting interparticle gaps after FSAM processing. The Al₂O₃ particles (14 µm) maintained their size, resulting in interparticle gaps of ~17 µm, while the MgB₂ agglomerates (1–140 µm) were broken down into smaller submicron particles during FSAM, leading to much finer interparticle gaps (<1 µm). This correlation highlights the FSAM process's ability to fragment larger agglomerates and refine particle distribution, especially for softer or clustered feedstock materials like MgB₂. Unlike the MgB₂ agglomerates, the Al₂O₃ particles have a more uniform shape with angular and elongated shapes. Their PSD is also narrower, spanning from 10 µm to 30 µm, and their d₅₀ is 13 µm (Fig. 1c, d). Figs. 1g and h show the metal components of the AMMC matrix, which consist of AA7075 (Al-6%Zn-Mg) powders with a PSD of 30-50 µm, AA7075

ingots, and pure aluminum powders with a PSD of 40-140 μm . Figs. 1e and f show the same results. Metal substrates, such as 5083 sheets and Al metal, both with a thickness of 5.0 mm, were used to construct the AMMCs using the stacked FSAM approach.

are used to create 46 mm thick AA7075/ Al_2O_3 AMMC sheets before the FSAM operation begins (Fig. 2a). The AA5083 substrate is then covered with the AA7075/ Al_2O_3 AMMC sheet. As shown in Fig. 2 (c), the FSAM operation involves inserting a friction stir tool into one end of the AA7075/ Al_2O_3 AMMC sheet.

Both solid-state powder metallurgy (PM) and liquid-state solidification procedures, including casting,



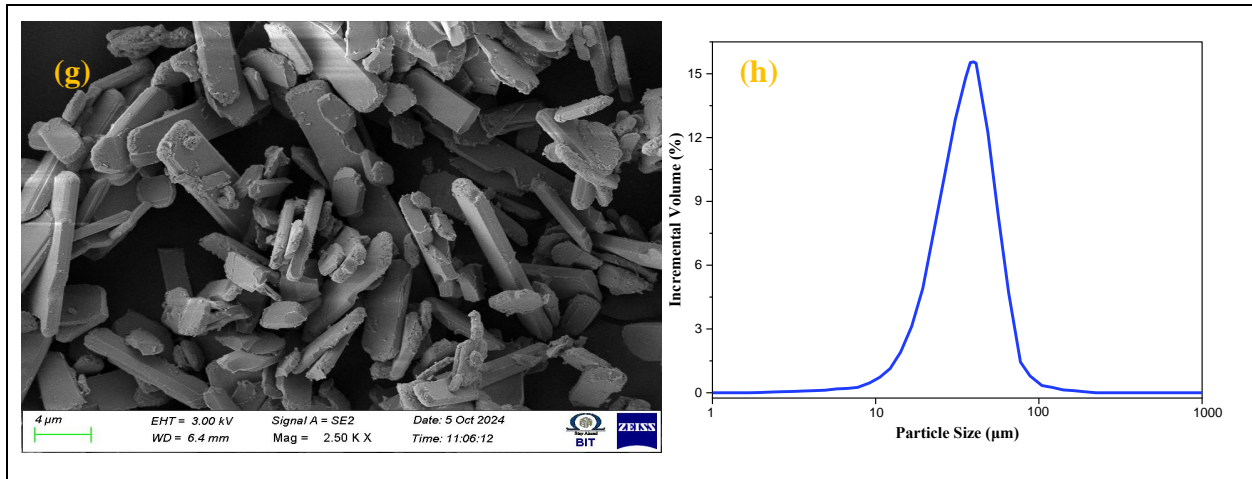


Fig. 1: (a, b) MgB₂, (c, d) Al₂O₃, (e, f) AA5083, and (g, h) AA7075 alloy nanoparticles of SEM images and PSD as-received

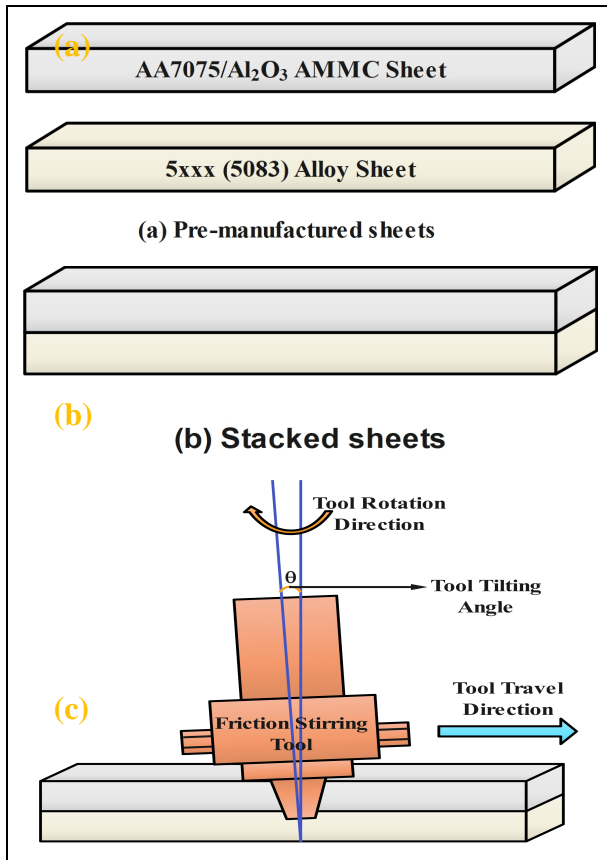


Fig. 2: An illustration of (a) the prior to the fabricated substrate, (b) the assembled substrate, and (c) the functioning of the stacking friction stir additive manufacturing progress

The tool is rotated at 500 to 1000 rpm and tilted at a vertical angle 3°. This process penetrates the surface of the underlying AA5083 substrate by approximately 1 mm. Then, after finishing one friction stir pass, the spinning stir tool continues to travel across the AA7075/Al₂O₃ AMMC sheet up to 200 mm/min speed. The entire AA7075/Al₂O₃ AMMC sheet is covered with

FSAM processes, creating multiple tracks that overlap and run parallel.

The composites made by the stacked FSAM have standard surface patterns and cross-sectional macro structures. To further compare the microstructures of FSAMs with AMMCs created using various fabrication processes, samples of AMMC were collected from stir-casting AA7075/Al₂O₃ nuggets and cold-sprayed AA7075/Al₂O₃ plates. The cold spray solid-state method comprises spraying a substrate with a fine-particle jet traveling at a speed of 300 to 1200 m/s. A supersonic gas stream drives powders into a heated nozzle, where the temperature is below their melting point. Pressurized inert gases drive the particles to supersonic speeds, then smash against surfaces at high enough pressure to produce either semifinished or finished items. Utilizing distinct powder feeders, AA7075 and Al₂O₃ powders were sprayed at a deposition rate of 2.71 g/min or lower to fabricate composites containing 20 vol% Al₂O₃. The AA7075/Al₂O₃ plate was fabricated using this method. Compared to spraying pure metal alloys, the deposition rate when incorporating a high percentage of ceramic nanoparticles into an MMC can be as much as 50% lower, highlighting the difficulties of the process.

A scanning electron microscope through ZEISS was employed to analyze the microstructure and morphologies of the AMMC samples. The metallic matrix and particles were analyzed elementally by combining SEM with energy-dispersive X-ray spectroscopy (EDS, Aztec, Oxford Instruments). The SEM pictures were analyzed using image analysis software (Image J) to evaluate the particle loading fraction from the area fraction. The evaluated area fraction should match the volume proportion for reinforcing particles like Al₂O₃ with faceted surfaces with relatively simple geometries. Image analysis software determines the interparticle distance using the linear intercept technique by establishing an arbitrary straight line on a scanning electron microscope (SEM),

enumerating the particles that intersect it, and then dividing the line length by the particle count and obtaining the average spacing between them. Averaging 10 readings yields the final value of the interparticle spacing.

Polished surfaces of these SEM samples were tested for micro-Vickers hardness (HV) with a 500 mN load using a microhardness tester (Micromet 2013, Buehler Ltd., IL, USA). The part of the AMMC samples that contained Al₂O₃ or MgB₂ and transitions from the Aluminum alloy substratum was a part that was measured.

In an ambient setting, a pin-on-disc tribometer was used for lubrication testing on dry sliding. Testing the AMMC materials' resistance to surface deterioration caused by frictional forces was the main objective of this tribological performance evaluation. Tungsten carbide (WC) with a hardness of up to 1600 HV was used to construct the corresponding pin, which had a diameter of 10 mm. Even though the MMC matrix is far more resilient than the Al₂O₃ particles—it has a hardness of 2,563 HV—the surface damage is more commonly seen on the surface of the specimen. Establishing a sliding velocity, weight, and sliding distance of 1 m/s, 3 N, and 150 m, respectively, was determined to assure the steadiness of the specimen and the reliability of the obtained data. All of the MMC samples were polished before sliding tribological testing to achieve a consistent surface roughness (Ra 1.1-1.3 μm), to reduce the impact of surface criteria on the results of the tests.

The proton radiation testing was performed on samples of AMMC disks measuring 25 mm × 9 mm × 1 mm. The 14UD Pelletron accelerator, which has doubled its units, was used for radiation testing. With a baseline pressure of 2.2 × 10⁻⁶ mbar, eight magnets with energies ranging from 15 to 25 MeV guided the testing samples to the target. A detector with an alumina surface blockade was positioned down to evaluate the energies transmitted through the samples. This study utilized the Stop and Range of ions in Matter (SRIM) to determine the Linear Transfer of Energy (LET) and mass of stop power (MSP) of metals and Aluminum Metal Matrix Composites (AMMCs). The software programs developed using experimental data are founded on nuclear interactions in the transport of matter involving ions and nuclei.

3. RESULTS AND DISCUSSION

3.1 Impact on the Addition of Nanoparticles

Nanoparticles in MMC comprise internally formed entities, such as eutectic aluminum particles and other minor inferior phases characteristic of the AA7075 alloy microstructural analysis, as well as externally injected materials, such as Al₂O₃ particles in AA7075/Al₂O₃ MMCs.

The impact of stacked FSAM on the quantity and dispersion of the incorporated Al₂O₃ particles compared to alternative fabrication techniques. The FSAM-produced AMMCs have more Al₂O₃ particles within the AA7075 alloy matrix, as demonstrated in Table 1. Particles such as eutectic Si, cast AA7075 alloy, and introduced Al₂O₃ constitute 45% of the total particles. According to Table 1, the interparticle spacing was determined at around 17 μm, and the distribution of both Al₂O₃ and additional particles was exceptionally even. FSAM MMCs offer high scalability, allowing the production of large thin-wall structures, whereas traditional MMCs (such as Stir Casting, Powder Metallurgy, and Cold Spray) are often limited to thick components. In terms of weight, FSAM MMCs maintain a low weight while offering better strength, whereas traditional MMCs have low to moderate weight. Regarding cost, FSAM MMCs are more efficient, minimizing waste and saving energy, making them a lower-cost option. Traditional MMCs, however, are high-cost due to energy-intensive processes and material waste. Performance-wise, FSAM MMCs demonstrate superior characteristics, including higher hardness, wear resistance, and radiation shielding. Traditional MMCs vary in performance, often being limited by processing challenges.

The commercial AMMC ingots made by liquid-state stir casting have a similar matrix interaction and Al₂O₃ particle loadings as the raw material. Still, they have 48 μm interparticle spacing because there are a lot of primary Al dendrites. In the spaces between dendrites, Al₂O₃ and Si particles clump together. Cold spray deposition AMMC's cannot obtain the maximum concentration of Al₂O₃ particles. Because many Al₂O₃ particles bounce back from the deposition surface when they engage with the deposited metal matrix composites, leading to minimum deposition rates, the cold-sprayed AMMC specimen had fewer than 20% Al₂O₃ particles.

These particles are distributed in the cold-sprayed specimen in a non-uniform manner, demonstrating segregation across strata of the aluminum alloys that may extend for several hundred micrometers. The interstitial space between Al₂O₃ particles is dictated by the initial dimensions of the aluminum particles and their elongation resulting from impact distortion through spray deposition. If deformation happens due to spray impact, the cold-sprayed AA7075/Al₂O₃ samples can have an interparticle spacing of 40-50 μm, the same as the 60 μm diameter of the Al alloy particles.

The stacking FASM process effectively provides a uniform distribution and high proportion of ceramic particles in AMMCs by using pure aluminium as the matrix and MgB₂ as the strengthening particles. The volume percentage of MgB₂ in the Al/MgB₂ can also exceed 30%, as demonstrated in Fig. 5, and their dispersion within the Al matrix is uniform, similar to the

AA7075/Al₂O₃ AMMCs (Table 1). According to Table 1, the proportion of MgB₂ particles that was measured is less than the aggregate fraction of Al₂O₃ and secondary particles (45%), but it is comparable to the fraction of Al₂O₃ particles (35%). The Al/MgB₂ sample exhibits an interparticle spacing of less than 1 μm for MgB₂, which is significantly lower than the 17 μm interparticle spacing observed for Al₂O₃ and other particles in the AA7075/Al₂O₃ composites (Table 1).

This notable decrease in interparticle spacing within the Al/MgB₂ composite correlates with a reduction in the dimensions of the incorporated MgB₂ particles from the as-received 14 μm (d₅₀), primarily attributable to substantial agglomeration, unlike the discrete particles observed in the Al₂O₃ feedstock. These MgB₂ clusters are broken up into submicron particles and particles measuring 1-5 μm, as shown in Fig.3. The scanning electron micrographs show that the nanoparticles are evenly dispersed throughout the aluminum matrix. (Prakash *et al.* 2023).

The volume fraction may be related to the measured area fraction of smaller particles because most of them have increased faceting. It appears from the EDS images in Fig. 3 that there are scattered particles that are rich in Mg or B, indicating that the as-received MgB₂ clusters include residual Mg metal. Because of its solid-state mixing activity, the FSAM process helps degum the MgB₂ clusters as they are received and reduces the space between the extra particles as they are added. The equitable distribution of these tiny particles within the matrix using FSAM significantly reduces the interparticle distance between the MgB₂ particles in the AMMC to less than 1 μm, as displayed in Fig 3. The size of Al₂O₃ is comparatively constant at 13 μm after FSAM processing, although the interparticle spacing is slightly reduced to 17 μm (Fig. 1c, d).

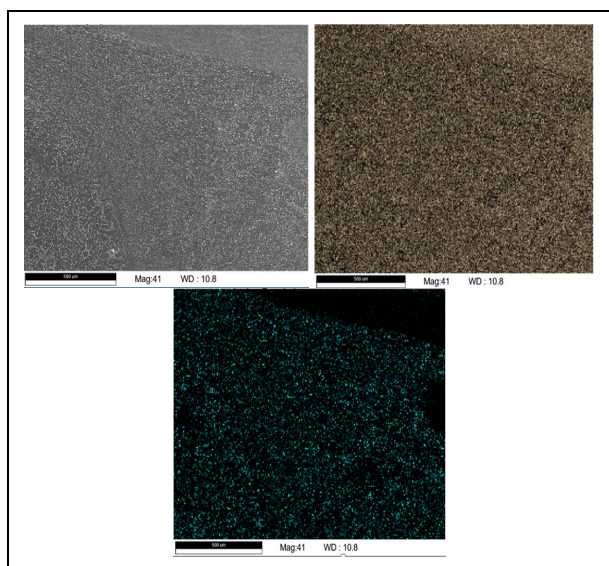


Fig. 3: EDS mappings of the AA7075/MgB₂ composite

Among other fabrication methods for AA7075/Al₂O₃ and Al/MgB₂ composites, the stacked FSAM process represents among the others for two main reasons: first, it can produce AMMCs devoid of segregation, coarse microstructures, and other defects; and second, it can improve interparticle spacing by redistributing secondary particles (in the case of AA7075/Al₂O₃) or by breaking up the introduced ceramic particles (in the case of Al/MgB₂), depending on the material. In addition to showing the dispersion of Al₂O₃ powder at the stir zone, the microstructural and morphological results of the laminated composite revealed refined and equiaxed grains (Prajapati *et al.* 2024).

The FSAM agitating instrument generates mass fluxes in the solid state, which is the source of the distinctiveness. Fig. 2c shows that the mass flows are made up of two parts: the vertical flows caused by the slanted rotating tool and the lateral flows caused by the stirring tool's horizontal movement. A more significant percentage of ceramic particles can be evenly mixed with a metal matrix if these fluxes move and mix the materials. The maximum ceramic-loading composites produced by liquid state stir casting techniques are susceptible to flaws including segregation, porosity, shrinkage, and fracture. Nonetheless, AMMCs produced by solid-state FSAM are devoid of defects. Multidirectional mixing of mass flows allows for the uniform distribution of ceramic particles, in contrast to other two-dimensional or linear solid-state processes such as rolling, extrusion, or deposition, which can lead to ceramic particles being segregated into bands or strata within the metal matrix. The significant deformation brought about by these mass fluxes during FSAM processing may also improve the metal matrix microstructures by disrupting primary, secondary, or additional particle clusters.

3.2 Impact of Elevated Ceramic Particle Concentration on Hardness and Friction Coefficient

Fig.4 illustrates the micro-Vickers hardness linked to 35% Al₂O₃ and MgB₂. The hardness of both materials increases to 180 HV due to the increased loading of ceramic particles. Fig.4 illustrates a sequence of hardness evaluations conducted within the cross-sectional view of the hybridized sheets. These data clearly show that the matrix is harder due to ceramic particles. The cross sections constitute an intermediate transition zone, a lower-quality aluminium/alloy substrate, and a higher-quality AMMC layer. The microhardness of the AA5083 substrate, which is devoid of any additional ceramic particles is approximately 115 HV in the hybrid sheet, illustrated in Fig. 4(a). It includes the AA7075/Al₂O₃ composite layer on top. In regions where the evolution from the aluminum alloy to the AMMC occurs, the hardness rises to 145-155 HV, coincident with an increase in the Al₂O₃ component. In

the upper section of the AMMC layer, the proportion of Al_2O_3 particles is approximately 35%, and the maximal recorded hardness is 175-185 HV. Microhardness gradients ranging from around 80 HV0.1 to approximately 145 HV0.1 were detected along the build depth in the successful production and characterization of a gradient composite microstructure composed of 3 mm thick sheets of AA5083-O, AA6061-T6, and AA7075-T6 (Jha and Imam, 2024)

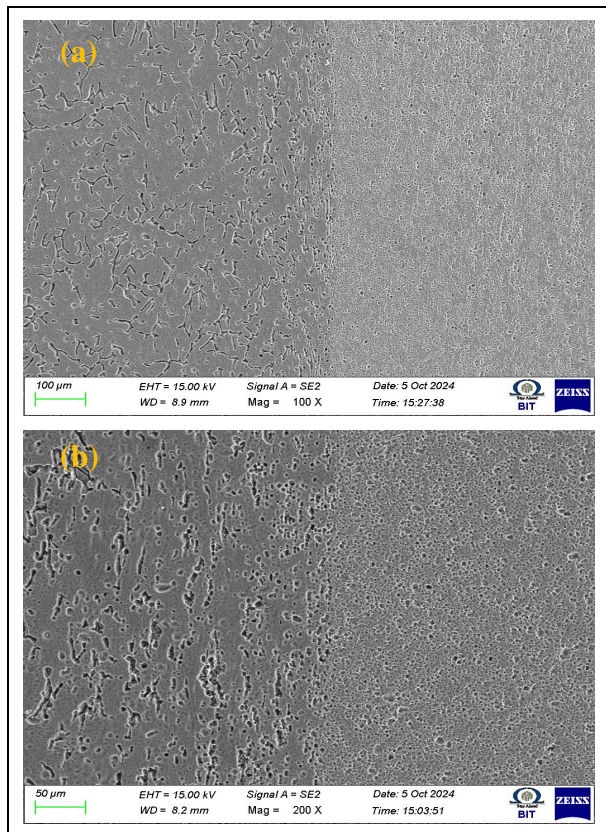


Fig. 4: SEM image of (a) AA7075/ Al_2O_3 and (b) AA5083/ MgB_2 on an aluminum metal substrate

A sequence of microhardness measurements over the cross-section of the hybridized sheet, which features an AA5083/ MgB_2 composite layer atop an Al substrate, is similarly illustrated in Fig.4(b). This sequence demonstrates an analogous rise in the hardness of Aluminum metal as an outcome of a substantial proportion of MgB_2 particles. The aluminum metal substrate has a hardness that ranges from 50 to 61 HV. The Al-to-AMMC transition area's voltage was subsequently elevated to more than 120 HV by adding MgB_2 nanoparticles. The recorded 181 HV at the midpoint of the AMMC layer indicates a MgB_2 component of approximately 35%. The Al/ MgB_2 composite layer's surface exhibited a maximal hardness of 214 HV.

The effects of a higher ceramic particle concentration on hardness and the association between

the ceramic fraction and the coefficient of friction (COF) are both explored in this study. This test aims to determine how well an AMMC surface can withstand the sliding of a more complex object, which could damage the protective layers of the aluminum substrate. Dry sliding experiments were performed on AA7075/ Al_2O_3 AMMC samples with a WC pin, as depicted in Fig.5. The findings demonstrate that the COF, indicative of the resistance force, escalates with the augmentation of Al_2O_3 particle fraction in the composites. When Al_2O_3 additions increase from 22% to 34%, the observed coefficient of friction increases by 85%. As the Al_2O_3 dosage rises from 22% to 34%, the mass loss of the AA7075/ Al_2O_3 sample is reduced from approximately 6 mg to less than 1 mg.

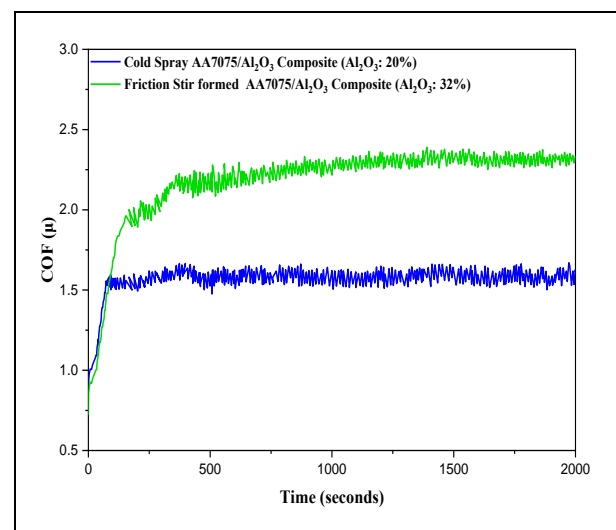


Fig. 5: Results of COF with varying Al_2O_3 loadings

The significant decrease in wear loss and marked improvement in hardness of these AA7075/ Al_2O_3 AMMCs, achieving levels equivalent to certain steels, can be ascribed to the high proportion of Al_2O_3 (exceeding 25%) uniformly dispersed within the metal matrix through FSAM, significant to a considerable reduction in inter-particle design, unlike the cold-sprayed AA7075/ Al_2O_3 samples with an Al_2O_3 fraction below 30% and a HV of 86HV (Table 1). The cold-sprayed AA7075/ Al_2O_3 samples exhibit a considerable 15% augmentation in the Al_2O_3 particle proportion. According to Table 1, the interparticle separation is significantly reduced to 17 μm due to the uniform mixing accomplished using the FSAM technique. In contrast, Table 1 shows that the coarse Al granules, which measure 40-200 μm in diameter, have an increased interparticle spacing owing to the segregation of Al_2O_3 particles in cold-sprayed AMMCs and a reduced proportion of Al_2O_3 particles (<20%). The wear test indicated that the particular wear rate diminished by approximately 63% with the addition of hybrid nano powder in the identical sample (Kiani and Mirsalehi, 2024).

The HV of both "softer" aluminum metal and "harder" alloy similarly increased, with the potential for the aluminum metal to achieve an even greater level of hardness by adding MgB₂. This finding suggests that, if the ceramic percentage exceeds 25%, further efforts to increase the hardness of the matrices have little impact on raising the total hardness of the AMMCs. Table 1 shows that a smaller MgB₂ interparticle spacing of less than 1 μm is more successful in increasing the AMMC hardness when the ceramic content in the AMMCs is consistent at 35%, compared to a greater Al₂O₃ interparticle spacing of around 18 μm. This conclusion is reinforced by the fact that the hardness of MgB₂, measured at 1,492 HV, is significantly inferior to that of Al₂O₃, which is 2571 HV, and that the total proportion of Al₂O₃ (35%) and secondary particles (15%) at 45% exceeds the fraction of MgB₂ within the matrix. To increase the hardness of AMMCs, it is more important to decrease the interparticle spacing than to increase the number of ceramic particles. The sample with an 80% filling density is excellent for powder filling in the MgB₂ superconducting tube, demonstrating the most significant critical temperature onset of 39.25 K. This sample yields the highest critical current density of 30 A/cm² (2T) (Herbirowo *et al.* 2024).

Table. 1 Evaluation of properties for AA7075/Al₂O₃ and Al/MgB₂ metal matrix composites

Specimen	Microhardness (HV)	Percentage of all particles of area Fraction	Percentage of added particles of area Fraction	All particles Interparticle spacing (μm)
AA7075/Al ₂ O ₃ FSAM	180 - 192	45 ± 2.5	40 ± 2.8	23 ± 3.3
AA7075/Al ₂ O ₃ Stir casting	99 ± 2.7	39 ± 4.6	29 ± 4.9	55 ± 13.6
AA7075/Al ₂ O ₃ Cold spray	86 ± 5.5	34 ± 4.4	25 ± 4.7	48 - 212
Al/MgB ₂ FSAM	191 ± 31	38 ± 1.3	35 ± 1.6	1.1 ± 0.13

3.3 Surface Damages and Proton Radiation: Space Hazard Mitigation in the Low-Earth-Orbit Environment

A unique and challenging area of additive manufacturing research is the production of next-generation radiation-resistant structural materials (Sun *et al.* 2021). Wear, impact, and heat resistance are all enhanced by using strong, high-melting-point ceramic particles. Some ceramics have exceptional structural and functional properties, like high melting points, hardness, and radiation attenuation. These characteristics are crucial to mitigate the impact of hazards in space, including ionizing radiation, severe temperature swings, and launch vibration. This research looks at AMMC materials with many ceramic particles to determine if they can mitigate surface degradation in a low-Earth orbit (LEO) setting caused by vibration and proton radiation.

Spacecraft and satellites are vulnerable to surface faults in their folding deployment mechanisms during launch. Because of the strong vibrations felt during takeoff, these systems can oscillate laterally (fretting) between a ball and a flat surface. This process removes the oxides and other naturally occurring protective layers from metal surfaces, exposing the "fresh" metal underneath. The coefficient of friction increases by 85% when the Al₂O₃ particulate loading is increased from 22% to 34%. A rise in the COF causes a more significant friction force to be required to resist the motion of a friction pair, given a fixed force at the interaction. A 22% to 34% rise in the particle loading of Al₂O₃ in the AMMCs results in an 85% rise in the resistance. So, movements can reduce their force, leading to less surface damage.

The proton radiation shielding studies, which compared MgB₂ reinforced composites to metals like magnesium and aluminum, took place in the energy between 12 and 16 MeV, a section of the proton energy spectra encountered in low Earth orbit (LEO) environments. The testing, shown as LET and MSP, is presented in Fig.6.

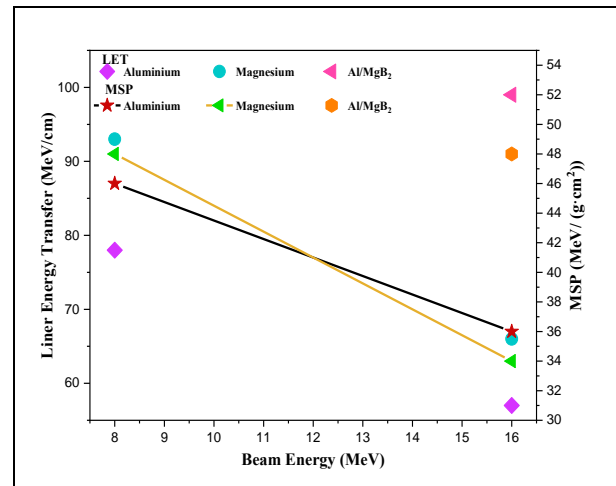


Fig. 6: Assessed linear energy transfer (LET) and mass stopping power of magnesium, aluminum, and the aluminum matrix composite (AMMC) including aluminum as the matrix and magnesium diboride (MgB₂) as the reinforcement (i.e., Al/Mg₂B)

For a given proton energy, the results show that the Al/MgB₂ sample outperforms the aluminum and magnesium metal specimens regarding LET and MSP by 20-40%. Fig.7 illustrated the findings of the SRIM calculation, which showed that compared to Al and Mg metals, the LETs of pure MgB₂ and Al/MgB₂ composites were higher. All energies were considered in the computation. Results from both experiments and calculations showed good agreement, since the LET/MSP of the Al/MgB₂ sample was greater than that of the aluminum and magnesium metal specimen. There is a significant discrepancy between the calculated and

observed LET improvements by MgB_2 in terms of absolute value and magnitude. Compared to the pure Al and Mg metals, the Al/MgB_2 sample exhibits LET and MSP readings that are 35–45% and 30–35% higher, respectively. However, there will be no discernible improvement.

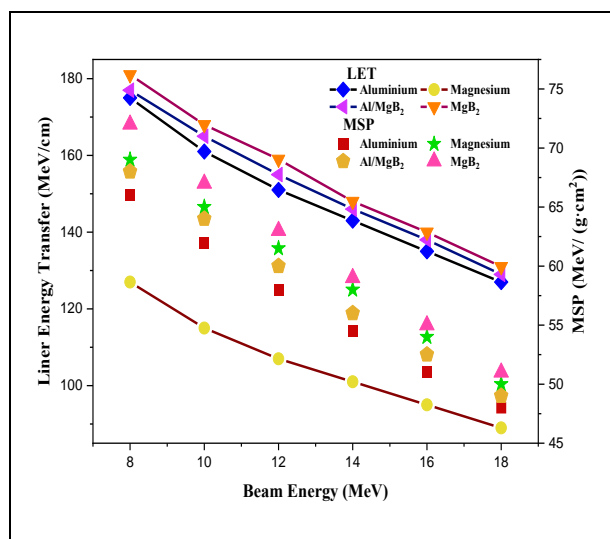


Fig. 7: LET and MSP of Mg, Al, MgB_2 , and the Al/MgB_2 AMMC sample determined using SRIM

The integration of MgB_2 significantly improves LEO radiation shielding, which goes against the conventional knowledge that proton ion radiation interacts with shielding materials. The dispersion and modification of particle radiation, particularly proton ions, have long been thought to be best accomplished by hydrogen. In conditions similar to those found in deep space, the efficient transfer of energy from proton ions in nuclear collisions is made possible by the H_2 nucleus, composed of only a proton with a mass equivalent to that of a proton ion. This is necessary since energy levels in these environments are routinely beyond 255 MeV. Using boron-containing materials in nuclear reactor shielding applications for spent nuclear fuel storage proves their ability to capture thermal neutrons. However, they do not exhibit the same level of scattering and modification as hydrogen-rich materials when it comes to emerging proton particle radiation.

Two factors are being considered in the ongoing investigation to identify prospective strategies for improving the shielding efficacy of MgB_2 . Such factors include the complicated electromagnetic structures of MgB_2 and the lower energy of LEO proton radiation. Energy loss is primarily due to proton ion collisions with shielding material nuclei, rather than electrons, reaching numerous 100 MeV. The electrical structures of shielding materials play a key role in energy transmission, might facilitate the presence of low-energy proton sources in the LEO environment. The second characteristic of MgB_2 is its unique layered architecture, characterized by a

complex electronic bonding configuration that alternates between boron and magnesium within the layers. As electronic structures evolve, shorter distances between Mg-Mg bonds are just one of many processes at function. Magnesium bifluoride's superconductivity stems from the bond structure that makes its electrical configuration susceptible to energy transmission by the vibrating crystal lattice, also known as phonons. More studies are needed to learn how electronic structures alter proton radiation at lower energy levels, which is essential for LEO radiation. The exceptional qualities of metal matrix composites based on aluminum, such as high strength, stiffness, corrosion resistance, fatigue resistance, wear resistance, etc., make them extensively applicable in aerospace, defense, marine, and space applications (Udayashankar and Ramamurthy, 2018).

4. CONCLUSION

To ensure that FSAM fabrication reaches advanced technological and production preparation levels, stacked friction stir additive manufacturing (FSAM) is used to create multifunctional AMMCs with a high proportion of ceramic particles (> 25%). Human dwellings, surface vehicles, spacecraft, and satellites are just a few of the many potentials uses for enhanced protective behavior in contradiction to the aviation environment risks and threats made possible by these AMMCs.

Adding uniformly distributed very hard ceramic particles to AMMCs like AA7075/ Al_2O_3 reduces the interparticle gap to dimensions close to the feedstock particle size and increases the hardness to levels similar to some steels. These AMMCs enhance the resistance to lateral motion at sliding contacts and reduce wear loss, enabling the folded deployment mechanisms to withstand launches with reduced surface damage.

A hybrid sheet can be created by integrating an Al/MgB_2 composite layer with an aluminium substrate to include favorable attributes, such as LEO proton radiation shielding, into these structural components. The effectiveness of the Al/MgB_2 composite in shielding LEO proton radiation is 30-20% higher than that of aluminium metal, as measured by linear energy transfer and mass stopping power. Further research is needed to understand how proton radiation interacts with the complex electronic structures of MgB_2 , improving radiation shielding effectiveness.

The stacked FSAM method enables the production of large-scale aluminium metal matrix composites with many functional particles. Titanium (Ti) alloys and other high-melting-point alloys need additional development before constructing MMCs. The key developments were wear-resistant tools (e.g., cBN), optimized process parameters (higher rotational/traverse speeds), thermal management (localized cooling/preheating), inert gas

shielding to prevent oxidation, and advanced material flow modeling. These improvements will enable defect-free, high-strength titanium MMCs for aerospace and space applications.

The friction stir additive manufacturing process incorporates numerous ceramics or intermetallic particles into titanium alloy metal matrix composites, exacerbating issues like alloy corruption and corrosion at elevated temperatures.

FUNDING

This research received no specific grant from any funding agency in the public, commercial, or not-for-profit sectors.

CONFLICTS OF INTEREST

The authors declare that there is no conflict of interest.

COPYRIGHT

This article is an open-access article distributed under the terms and conditions of the Creative Commons Attribution (CC BY) license (<http://creativecommons.org/licenses/by/4.0/>).



REFERENCES

- Aydogan, E., El-Atwani, O., Erdem, B., Chen, W. Y., Li, M., Devaraj, A., Koc, B. and Maloy, S. A., In-situ radiation response of additively manufactured modified Inconel 718 alloys, *Addit. Manuf.*, 51, 102601 (2022). <https://doi.org/10.1016/j.addma.2022.102601>
- Bhattacharjee, R., Datta, S., Medhi, T. and Biswas, P., Friction Stir Welding and Its Advancement, In: Sustainable Smart Manufacturing Processes in Industry, 4, 183–220 (2023), <https://doi.org/10.1201/9781003436072-10>
- Bülbül, F. and Kara, A., Multifunctional electroless nickel boron composite coatings incorporated by magnesium diboride ceramic particles, *Int. J. Ceram. Eng. Sci.*, 6(6), 1-13 (2024). <https://doi.org/10.1002/ces2.10237>
- Chakrabarty, S., Thakur, A., Rasyotra, A., Gaykwad, B. and Jasuja, K., Quasi-Two-Dimensional Nanostructures from AIB₂-Type Metal Borides: Physicochemical Insights and Emerging Trends, *J. Phys. Chem. C*, 127(2), 852–870(2023). <https://doi.org/10.1021/acs.jpcc.2c07070>
- Choudhury, S., Acharya, U., Roy, J. and Roy, B. S., Recent progress in solid-state additive manufacturing technique: Friction stir additive manufacturing, *Proc. Inst. Mech. Eng., Part E: J. Process Mech. Eng.*, 237(2), 467–491 (2023). <https://doi.org/10.1177/09544089221107755>
- Das, A., Biswas, P. and Kapil, S., Influence of Friction Stir Additive Manufacturing Parameters on Dry Friction and Wear Properties of Al-Mg-Si Alloy's Built Surfaces Fabricated by Sheet Lamination, *J. Tribol.*, 146(5), 1-13(2024). <https://doi.org/10.1115/1.4064303>
- Hawkins, L., Yang, J., Song, M., Schwen, D., Zhang, Y., Shao, L., Lou, X. and He, L., The effect of secondary phases on microstructure and irradiation damage in an as-built additively manufactured 316 L stainless steel with a hafnium compositional gradient, *J. Nucl. Mater.*, 587, 154708 (2023). <https://doi.org/10.1016/j.jnucmat.2023.154708>
- Herbirowo, S., Marlina, H. A., Elita, K., Pham, A. T., Tran, D. H., Putri, W. B. K. and Imaduddin, A., A comprehensive analysis of MgB₂ superconducting wire development: The effect of initial filling density and thermomechanical treatment, *Case Stud. Chem. Environ. Eng.*, 10, 1-8 (2024). <https://doi.org/10.1016/j.cscee.2024.100970>
- Herbirowo, S., Priyanto, U. E., Feronika, T. D., Sinuhaji, P., Sofyan, N., Herman, Y. A. and Imaduddin, A., Properties of low-cost MgB₂ superconducting wires fabricated by high reduction cold rolling, *Mater. Today Proc.*, <https://doi.org/10.1016/j.matpr.2023.01.250>
- Jha, K. K., Kesharwani, R. and Imam, M., Numerical and Experimental Study on the Effect of Tool Pin Profile of Friction Stir Additive Manufactured AA6061/AA7075 Joints, *Springer Proc. Mat.*, 52, 85–101 (2024). https://doi.org/10.1007/978-981-97-5959-0_6
- Jha, K. K., Kesharwani, R. and Imam, M., Microstructure, texture, and mechanical properties correlation of AA5083/AA6061/SiC composite fabricated by FSAM process, *Mater. Chem. Phys.*, 296(2023a). <https://doi.org/10.1016/j.matchemphys.2022.127210>
- Kiani, S. and Mirsalehi, S.E., Friction stir additive manufacturing of B₄C and graphene reinforced aluminum matrix hybrid nanocomposites using consumable pins, *J. Mater. Res. Technol.*, 28, 1094–1110 (2024). <https://doi.org/10.1016/j.jmrt.2023.12.065>
- Kiani, S., Mirsalehi, S.E. and Sahraei, A., Linear and cylindrical friction stir additive manufacturing (FSAM) of AA6061-T6 by consumable rods: metallurgical structure, wear, and corrosion properties, *Weld. World*, 68(11), 2869–2889 (2024). <https://doi.org/10.1007/s40194-024-01839-w>

- Kundurti, S. C. and Sharma, A., Evaluation of Microstructural, Mechanical and Corrosion Behaviours of Laminated AA6061/AA7075 Metal Matrix Composites Build by Friction Stir Additive Manufacturing for Structural Applications, *Mat. Res.*, 26 (2023). <https://doi.org/10.1590/1980-5373-MR-2023-0176>
- Lopez, J., Cerne, R., Ho, D., Madigan, D., Shen, Q., Yang, B., Corpus, J., Jarosinski, W., Wang, H. and Zhang, X., In Situ Reactive Formation of Mixed Oxides in Additively Manufactured Cobalt Alloy, *Mater.*, 16(10), 3707 (2023). <https://doi.org/10.3390/ma16103707>
- Lu, Q., Han, W., Deng, J., Li, H. and Wei, Z., Modular gas-cooled reactor core optimal design and additive manufacturing performance based on SiC matrix dispersed with TRi-structural ISOTropic fuel, *Energy*, 308, 132837 (2024). <https://doi.org/10.1016/j.energy.2024.132837>
- Nallusamy, M., Suriyaprakash, M., Kiran, K. and Jayachitra, M., Microstructural Analysis and Mechanical Properties of Three-Layered Stack of FSAM AA7075-Cu Alloys, *Surf. Rev. Lett.*, 31(1), 24500069 (2024). <https://doi.org/10.1142/S0218625X24500069>
- Pal, Y., Palateerdham, S.K., Mahottamananda, S.N., Sivakumar, S. and Ingenito, A., Combustion performance of hybrid rocket fuels loaded with MgB₂ and carbon black additives, *Propul. Power Res.*, 12(2), 212–226 (2023). <https://doi.org/10.1016/j.jprr.2022.11.003>
- Prajapati, R., Dwivedi, S., Kumar, D., Srivastava, A. K. and Dixit, A. R., Investigation on Bonding Strength and Tribological Performances of Ceramic Laminated AA6063 Composite Developed by Friction Stir Additive Manufacturing, *Int. J. of Precis. Eng. and Manuf.-Green Tech.*, 11(1), 89–105 (2024). <https://doi.org/10.1007/s40684-023-00545-0>
- Prakasam, M., Balima, F., Noudem, J. and Largeteau, A., Dense mgb₂ ceramics by ultrahigh pressure field-assisted sintering, *Ceramics*, 3(4), 521–532 (2020). <https://doi.org/10.3390/ceramics3040042>
- Prakash, J. U., Jebarose Juliyana, S., Salunkhe, S., Gawade, S. R., Nasr, E. S. A. and Kamrani, A. K., Mechanical Characterization and Microstructural Analysis of Stir-Cast Aluminum Matrix Composites (LM5/ZrO₂), *Crystals*, 13(8), 1220 (2023). <https://doi.org/10.3390/cryst13081220>
- Sharifzadeh, M., Bani Mostafa Arab, N. and Refahi Oskouei, A., The impact of friction stirs additive manufacturing parameters on the hardness and wear resistance of aluminum-silicon carbide nanocomposite, *Int. J. Interact. Des. Manuf.*, 19, 1971–1986 (2024). <https://doi.org/10.1007/s12008-024-01921-z>
- Srivastava, M., Rathee, S., Maheshwari, S., Noor Siddiquee, A. and Kundra, T. K., A Review on Recent Progress in Solid State Friction Based Metal Additive Manufacturing: Friction Stir Additive Techniques, *Crit. Rev. Solid State Mater. Sci.*, 44(5), 345–377 (2019). <https://doi.org/10.1080/10408436.2018.1490250>
- Sun, Z., Xu, Y., Chen, F., Shen, L., Tang, X., Sun, L., Fan, M. and Huang, P., Effects of ion irradiation on microstructure of 316L stainless steel strengthened by disperse nano TiC through selective laser melting, *Mater. Charact.*, 180, 111420 (2021). <https://doi.org/10.1016/j.matchar.2021.111420>
- Tagimalek, H. and Mahmoodi, M., Evaluation of wear test on functionally graded metal-polymer tri-laminate composite interfaces of cooling-assisted friction stir additive manufacturing, *J. Adv. Joining Processes*, 8, 1-12(2023). <https://doi.org/10.1016/j.jajp.2023.100166>
- Tan, Z., Li, J. and Zhang, Z., Experimental and numerical studies on fabrication of nanoparticle reinforced aluminum matrix composites by friction stir additive manufacturing, *J. Mater. Res. Technol.*, 12, 1898–1912 (2021). <https://doi.org/10.1016/j.jmrt.2021.04.004>
- Udayashankar, S. and Ramamurthy, V. S., Development and characterization of Al6061-Zirconium dioxide reinforced particulate composites, *Int. J. Eng. Tech.*, 7(3), 128–132(2018). <https://doi.org/10.14419/ijet.v7i3.12.15901>
- Venkit, H. and Selvaraj, S. K., Novel Technique for Design and Manufacture of Alternating Gradient Composite Structure of Aluminum Alloys Using Solid State Additive Manufacturing Technique, *Mater.*, 15(20), 1-21 (2022). <https://doi.org/10.3390/ma15207369>